



Research Article

Nb-Doped TiO₂ Photocatalysts Used to Reduction of CO₂ to Methanol

M. V. Nogueira ¹, G. M. M. Lustosa,¹ Y. Kobayakawa,² W. Kogler,³ M. Ruiz,¹
E. S. Monteiro Filho,¹ M. A. Zaghete,¹ and L. A. Perazolli ¹

¹Instituto de Química de Araraquara, UNESP, Araraquara, SP, Brazil

²Tokyo University of Science, Tokyo, Japan

³Friedrich-Alexander University Erlangen-Nürnberg, Erlangen, Germany

Correspondence should be addressed to M. V. Nogueira; tcep1@hotmail.com

Received 13 June 2017; Revised 26 September 2017; Accepted 15 October 2017; Published 2 April 2018

Academic Editor: Fernando Lusquiños

Copyright © 2018 M. V. Nogueira et al. This is an open access article distributed under the Creative Commons Attribution License, which permits unrestricted use, distribution, and reproduction in any medium, provided the original work is properly cited.

In pursuit of higher photoactivity, Nb-doped TiO₂ powders were evaluated in the reduction of CO₂. The replacement of Ti by Nb in the crystalline structure of TiO₂ promoted methanol formation. Nb-doped TiO₂ powders were successfully synthesized in Nb concentrations of 0.0, 0.5, 1.0, and 2.5% (w/w = weight/weight) using the Pechini method. The materials were calcined at 500°C for two hours to promote the formation of the anatase crystalline phase. After characterization, the powders were modified through an Nb⁰ magnetron sputtering deposition using a metallic target in vacuum conditions of 2×10^{-3} torr, with a deposition time of 10 minutes, and calcination again at 500°C for two hours. The resulting powders showed a surface area up to 30 m²/g. The Pechini method promoted the substitution of Ti⁴⁺ for Nb⁴⁺ as observed using XRD and XPS techniques at the crystalline structure and at the surface of the powder. Furthermore, the presence of Nb⁰ was also observed at the powder's surface. The presence of Nb in the crystalline structure increased the photoactivity of powders when compared to nonmodified TiO₂ powders, while the Nb⁰ deposition at the powder's surface decreased the photoactivity for all the investigated compositions.

1. Introduction

The development of photocatalysis began in 1972 [1], aiming to create efficient water treatment systems and to produce H₂ to use as fuel. Various researchers have conducted investigations in many different fields, such as semiconductor photoelectrochemistry [2], photocatalysis [3, 4], and photoreduction of CO₂ in aqueous environments, to produce methanol [5]. The TiO₂ produced by Evonik, known as TiO₂-P25 (consisting of 75% anatase phase and 25% rutile phase), is the mostly used for this purpose due to its excellent photoactivity and is also used as a reference to compare results with others news materials. TiO₂-P25 has high surface area (~50 m²/g), and its complex crystalline microstructure is directly related to the synthesis method [6].

The photocatalysis process consists in the exposition of semiconductor powder to ultraviolet light radiation which will create then the electron-hole pair from the electronic excitation. The hole (h⁺) is formed in the valence band, and

the electrons (e⁻) are formed in the conduction band. These species can react with adsorbed water or hydroxyl group and produce hydroxyl (OH^{*}) radical and superoxide anion (O₂^{*-}) radical, starting an oxidation and reduction process and then degrading the component of interest [7–9].

The addition of transitional metals to TiO₂ seeks to increase the recombination time of electron/hole pair during electronic excitation [10, 11]. It is believed that these transitional metals create acceptor/donor electron centers, influencing the electronic recombination. Perazolli et al. [12] synthesized a ternary mixture of Ti, Sn, and Ag oxides that obtained better Rhodamine B discoloration results than P25 due to the heterojunction TiO₂/SnO₂ and formation of metallic Ag reduced from Ag₂O increasing the recombination time. The utilization of heterostructures has been studied in degradation of organic compounds. Through the solvothermal synthesis, Li et al. [13] synthesized pure anatase, pure rutile, and mixed anatase-rutile cake-like particles and observed that anatase-rutile particles reached

higher photocatalytic activity compared to powders of pure phases (anatase and rutile) and also higher than P25. In the work of Zhou et al. [14], heterostructures of CdS/TiO₂ were synthesized in different concentrations (wt.) of CdS and then used in degradation of methyl orange dye. It was observed that the photocatalyst of concentration 2% (wt.) reached total degradation of dye in 75 minutes, a higher activity when compared to pure TiO₂ that reached only 90% of degradation at the same time, showing that the hetero-junction promotes better charge separation and increases the recombination time of electron-hole pairs (e⁻/h⁺). Through the hydrothermal synthesis, Tao et al. [15] deposited the heterostructures of TiO₂/ZnO/Ag on FTO substrate where Ag⁰ acts like antennae capturing the electrons photogenerated and then increased the recombination time for improving the degradation of methyl orange dye. The photocatalyst TiO₂/ZnO/Ag reached 96% of degradation of dye in 120 minutes, better than the results of pure TiO₂ (46%) and of TiO₂/ZnO heterostructure (62%) at same conditions.

Research of efficient processes in the conversion of CO₂ into methanol, ethanol, CH₄, H₂, and other compounds has been made since the late 1980s [16]. The use of Pd as a dopant in TiO₂ was evaluated on CO₂ hydrogenation under UV irradiation generating the amount of 355.62 μmol CH₄/g-cat by the increase of recombination time of generated electrons and adsorption and activation of CO₂ molecules on surface of catalyst [17]. Cheng et al. [18] used Cu²⁺-TiO₂ nanorod thin film photocatalysts reducing CO₂ into methanol and ethanol obtaining, respectively, 36.18 μmol/g-cat-h and 79.13 μmol/g-cat-h in which Cu²⁺ acted as active sites of electron traps and could suppress the electron-hole recombination allied to high surface area of TiO₂ nanorods. Pan et al. [19] produced Pt nanoparticle-dispersed gallium oxide (Pt/Ga₂O₃) catalysts calcined in different atmospheres at 600°C in comparison with Pt/P25; the oxygen vacancies promoted better CO₂ adsorption leading more efficient separation of the photo-induced electron-hole pairs and reaching 2.1 and 1.9 μmol CH₃OH using Pt/Ga₂O₃ and Pt/P25, respectively.

The use of a substituent that has a higher electron valence number than Ti⁴⁺, as Nb⁵⁺ an example, can lead to a level of electron donation that behaves like an extrinsic n-type semiconductor, which can act in the photoreduction reaction. One way to introduce the elements of the TiO₂ ceramic matrix in order to improve the photocatalytic properties by substitution of Ti⁴⁺ cation for Nb⁵⁺ is the chemical synthesis through Pechini's method. This method is useful to obtain ceramic powders since it is possible to control parameters as composition and crystalline phase through the immobilization in a complex organic matrix and controlled calcination, decreasing the segregation of metals and then providing homogenous distribution of the components [20, 21]. The sputtering method is a powerful tool of deposition of metals on surfaces and can be used in superficial modification of catalysts improving optical and electrical properties [22, 23].

Brazil has the biggest reserve of niobium of the world, possessing 98% of world niobium ore reserves [24]. This

work chose niobium due to the abundance and low cost of niobium (Nb₂O₅, Nb⁰) allied with the advantages brought with the structural modification by doping (n-type extrinsic semiconductor/excess of electrons and defects generation) and superficial modification (oxygen vacancies and formation of antennae) both improving charge separation and increasing the electron-hole pair recombination time. The goal of this research was to synthesize and characterize TiO₂-based photocatalytic powders modified with Nb in two ways: into the crystalline structure Nb⁴⁺ (by chemical synthesis Pechini) and upon the surface Nb⁰ (through sputtering deposition), as well as aiming at improving the photocatalyst properties by combining these two methods (the novelty). The concentration of dopants from 0.0 to 2.5% (w/w) was adopted to guarantee the formation of a solid solution and avoid the appearance of other phases [25]. It also intended to verify the photocatalytic activity of these powders in the reduction of CO₂ to methanol.

2. Experimental

2.1. Synthesis of Photocatalytic Powders. In this work, we prepared two polymer precursor solutions through the Pechini method:

- The titanium polymeric solution was obtained by slow addition of titanium isopropoxide (Aldrich) in ethylene glycol (Synth) at 80°C with constant stirring, then the heating was raised to 110°C, and the citric acid (Carlo Erba) was added. The molar ratio for the preparation of this stock titanium solution was 1 : 4 : 16 (metal : citric acid : ethylene glycol).
- The niobium polymeric solution was obtained by dissolution of niobium oxide (Nb₂O₅) (Carlo Erba) in hydrofluoric acid aqueous solution under stirring and heating (80°C). The pH of the solution was increased to 8 by addition of ammonium hydroxide (Synth), causing precipitation as hydroxide of niobium [Nb(OH)₅]. The precipitate was washed with distilled water to eliminate fluoride ions (F⁻) until the test with calcium carbonate (CaCO₃) to give negative fluoride ions. The niobium hydroxide was dissolved in aqueous solution of citric acid under stirring and heating (±80°C), followed by addition of ethylene glycol. The molar ratio for the preparation of stock niobium solution was 1 : 4 : 16 (metal : citric acid : ethylene glycol) [26]. The niobium and titanium solutions were standardized gravimetrically at 900°C for 2 hours.

After preparation of polymeric solutions, new solutions were obtained from the mixture of the previously prepared solutions according to addition of niobium: 0, 0.5, 1, and 2.5% (w/w) and then submitted to calcination in a muffle furnace at 500°C for 1 hour and milling by 500 rpm for 1 hour.

For superficial decoration by deposition of Nb⁰ through sputtering, circular pellets of 1.0 g of each powder were prepared using a hydraulic press (BOVENAU-P15500) applying a load of 2500 kg for 5 minutes and then introduced into the deposition chamber of sputtering (Sorensen DCS 600-1.7) for deposition according to the following conditions:

metallic spherical target of niobium, time of deposition of 10 minutes, vacuum of 2×10^{-3} torr with argon gas plasma, potential of 370 V, and a current of 0.055 A [27]. The pellets were macerated into powders again and submitted to heat treatment at 500°C for 1 hour promoting a more effective adhesion of the metallic Nb particles on TiO₂ surface obtaining the powders modified superficially by sputtering.

2.2. Sample Characterization. The powders were analyzed utilizing TGA/DTA (Netzsch Thermische Analyse-STA 409) to evaluate the temperature in which all organic matter can be removed. Furthermore, phase transits from anatase to rutile could be detected using this method.

In order to investigate the crystallinity of the material and identify the present phases, X-ray Diffraction (XRD) and the Rietveld method (XRD-Rigaku Rint-2000) with radiation source of copper emission line (Cu K α , $\lambda = 0.154$ nm) and voltage acceleration of 42 kV, 120 mA current, and scan rate of $2\theta \text{ min}^{-1}$ were used.

The Raman spectroscopy was adopted to evaluate the different phases present in the powders utilizing HORIBA-HR 800, with laser 632.8 nm. Infrared spectroscopy measurements were made in Shimadzu FTIR 8300 using the transmission technique (resolution: 4 cm^{-1} , spectral range: 4000 to 400 cm^{-1} , and 50 scans). The XPS technique (UNISPECS UHV) was used to analyze surface changes in the chemical composition due to the substitution to Nb.

The spectrophotometer Varian Cary model 500 was used for quantification of the bandgap values. The SBET technique was used to verify the specific surface area (Micrometrics ASAP 2010). The particle size of the powder and its morphology were evaluated in a field emission scanning electron microscopy (FE-SEM JEOL 7500F model).

2.3. Photocatalytic Activity. The photocatalytic activity of reduction was carried in a reactor (Heraeus) made out of quartz tube housing for the cooling of the mercury UV lamp of 150 W. In this reactor, a magnetic stirrer, a CO₂ bubbling tube, an inlet and outlet for water cooling, and a sample collector tube were coupled as illustrated in Figure 1.

The volume of 700 mL of deionized water was used, and the pH was increased to 12 with NaOH. Previously a blank test (photolysis) was made using no photocatalyst, and posteriorly in each solution, 0.350 g [28] of each photocatalytic powder was added and the reactions had the duration of 6 hours with removal of aliquots every 30 min that were analyzed through gas chromatography (GC-FID) in the chromatograph Varian CP-3800 with a flame ionization detector in column (Stabilvax-Restec 30 m, 0.25 mm inner diameter) using the technique SPME (solid phase micro-extraction) that adsorbs volatile organic compounds of aqueous samples on fiber (75 μm Carboxen/PDMS, SUPELCO) by heating (headspace method) and flow rate N₂ $1.0 \text{ mL} \cdot \text{min}^{-1}$. To quantify the methanol in the samples, aliquots of 0.5 mL were transferred to 1.5 mL vial and heated for 7 minutes, then the fiber was exposed to the vapor formed for 5 minutes to promote desorption, and finally, the fiber was injected into GC.

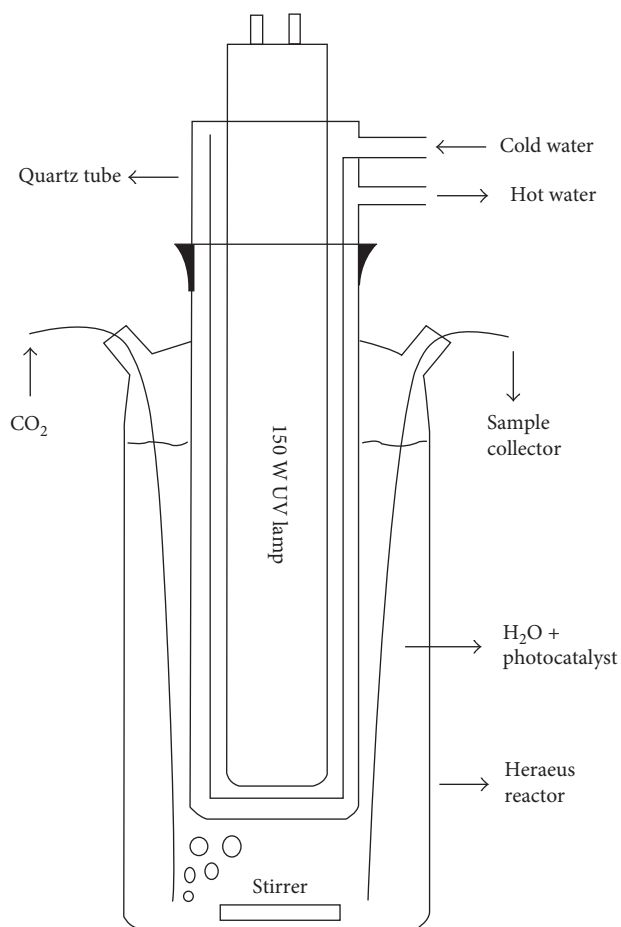


FIGURE 1: Design of the photocatalytic reactor.

3. Results and Discussion

3.1. TG/DTA Characterization. Figure 2 showed the results from the photocatalytic powder Nb-TiO₂ with 2.5% Nb (w/w). The TG curve of the precalcined powder ("puff") Nb-TiO₂ with 2.5% Nb (w/w) showed a weight loss at two distinct times. The first loss occurred between 30°C and 120°C and represented 4% of the initial weight and was attributed to water loss. The second loss, 40% of initial weight, was observed between 250°C and 480°C and was attributed to the calcination of organic precursors (citrate). There was no significant mass variation over 500°C. The DTA curve showed two significant thermal events, represented at first by an endothermic peak of around 100°C and characteristic of dehydration of the sample, and secondly by an exothermic peak at 413°C, attributed to the decomposition of organic matter. Therefore, in this experiment, the final temperature of 500°C was adopted because it guarantees total elimination of organic matter in the powders.

3.2. XRD and Rietveld Characterization. The XRD (Figure 3) indicates that the photocatalytic powders are mainly made of the anatase crystalline phase in comparison to characteristic peaks reported in the standard (R) JCPDS-73-1764. However, a peak at $2\theta = 27.5^\circ$, characteristic of the rutile crystalline phase, was observed. This confirms their presence due

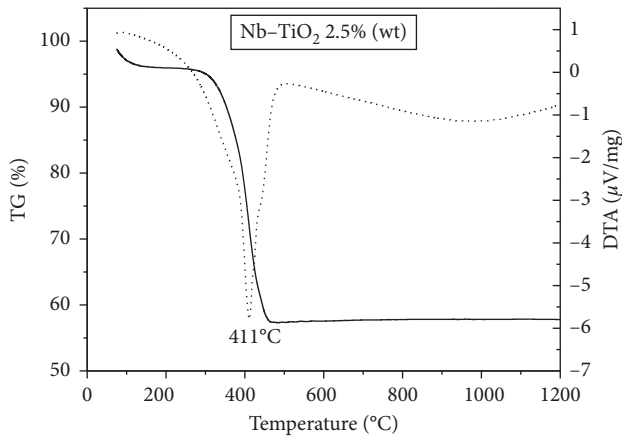


FIGURE 2: TG/DTA curves of precalcined TiO_2 photocatalyst Nb- TiO_2 2.5% Nb (w/w).

to the applied calcination temperature of 500°C , which is sufficient to cause partial phase transition to the rutile phase.

Another fact observed in the XRD patterns was the gradual shrinkage of all of the peaks with increase of Nb concentration in TiO_2 powder, attributed to the substitution of Nb in the TiO_2 crystalline lattice. Thus, considering the peak $2\theta = 48^\circ$ plane (2 0 0), it is found that the surface modification did not change the results obtained by XRD. Another effect observed by increasing the concentration of Nb was the leftward shift of the $\Delta 2\theta'$ peaks. These were justified by the distortion in the crystalline TiO_2 lattice generated by vacancies, interstitials, and substitutions [10] and by the difference of cationic rays in Ti^{4+} (0.74 \AA) substituted by Nb^{4+} (0.82 \AA), which reinforces the results observed in the TG/DTA analysis described previously.

Figure 4 illustrates the refined XRD pattern through the Rietveld method which can be observed beyond the XRD curves. The overlapping calculated setting curves show the positions of the Bragg peaks in the rutile and anatase crystalline phases in the samples and, further below, the residual adjustments.

The results obtained by Rietveld and shown in Table 1 indicate that the percentages of the anatase phase increased from 91.76% to 98.27% in photocatalytic powders Nb- TiO_2 0.0% (w/w) and Nb- TiO_2 2.5% (w/w), respectively. The percentage of the rutile phase decreased from 8.24% to 1.73%, indicating that the increase in the concentration of Nb in the photocatalytic powders acts as a rutile phase inhibitor.

Considering the change in values of cell parameters (a , b , c) of anatase and rutile crystals that was caused by the replacement of Ti for Nb and comparing them to the Nb- TiO_2 photocatalyst 0.0% (w/w), which does not contain Nb, it was observed that there is a decrease in cell volume ranging from 133.74 \AA^3 to 133.53 \AA^3 in Nb- TiO_2 0.5 Nb% (w/w) and Nb- TiO_2 2.5% Nb (w/w), respectively. This implies that Nb substituted in octahedral sites of this phase promotes the compression of the individual cell.

3.3. IR and Raman Characterization. The results obtained by IR spectroscopy (Figure 5) indicated that the photocatalytic powders show characteristic bands (3450 and 1640 cm^{-1})

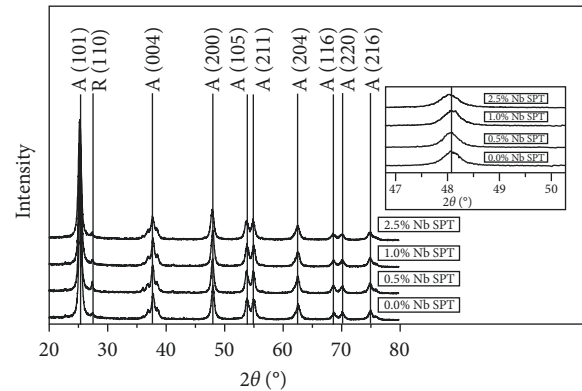


FIGURE 3: XRD patterns of photocatalytic powders modified by deposition of Nb^0 through sputtering (SPT) compared to the standard TiO_2 rutile (R) JCPDS 78-1510 and TiO_2 anatase (A) JCPDS 73-1764. Detail: $2\theta = 48^\circ$ plane (2 0 0) anatase.

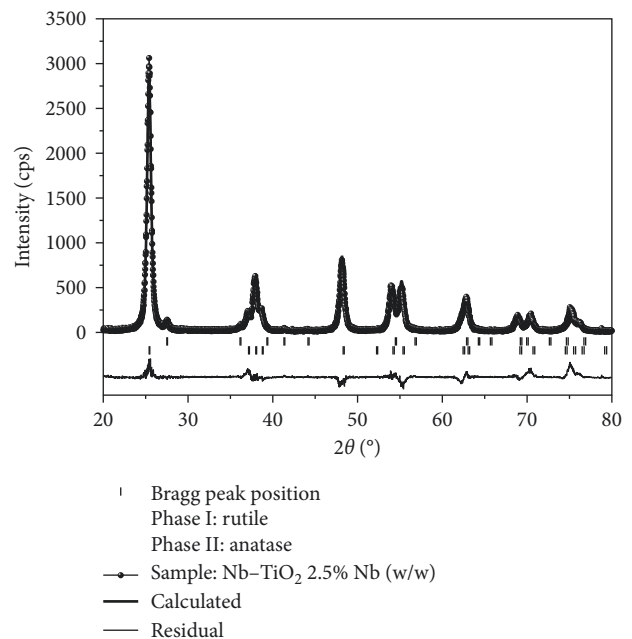


FIGURE 4: XRD diffractogram refined by the Rietveld method for the photocatalyst powder Nb- TiO_2 2.5% Nb (w/w) without modification by deposition of Nb^0 through sputtering.

attributed to the presence of water in atmospheric humidity. The O-Ti-O bonds are attributed to strong band at 979 cm^{-1} and the Ti-O-Ti bonds to weak band at the range of $800\text{--}465 \text{ cm}^{-1}$. These bands are characteristics of the TiO_2 -based photocatalysts. It was also observed that the presence of CO_2 at 2349 and 1337 cm^{-1} and CO at 2070 cm^{-1} is due to the capacity of the photocatalytic powders to adsorb some compounds that come from the decomposition of organic precursors present in the “puff,” adsorbed in the calcination process. The comparison of the photocatalytic powders and commercial anatase TiO_2 powder in IR analysis confirms that all organic matter was eliminated after heat treatment.

Figure 6 illustrates the Raman spectra of the photocatalytic powders. It is possible to notice that the characteristic

TABLE 1: Anatase/rutile percentages and unit cell parameters calculated for the powders.

Photocatalyst (% Nb (w/w))	Percentage		Cell parameter							
	Anatase	Rutile	Anatase			Rutile			Cell volume (\AA^3)	
			a	b	c	a	b	c	Anatase	Rutile
Nb-TiO ₂ 0.0	91.76	8.24	3.770	3.770	9.477	4.580	4.581	2.951	134.74	61.95
Nb-TiO ₂ 0.5	94.90	5.10	3.762	3.762	9.445	4.582	4.582	2.952	133.70	61.99
Nb-TiO ₂ 1.0	97.74	2.26	3.760	3.760	9.446	4.589	4.589	2.943	133.58	62.00
Nb-TiO ₂ 2.5	98.27	1.73	3.759	3.759	9.446	4.581	4.581	2.955	133.53	62.04

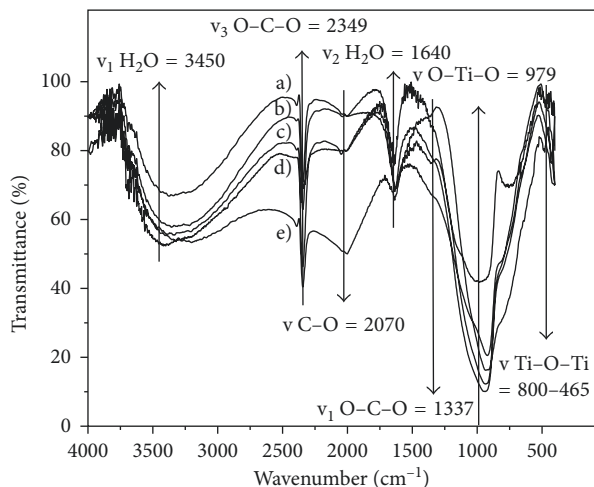


FIGURE 5: IR spectra of photocatalytic powders compared to commercial TiO₂ anatase Synth powder: (a) Nb-TiO₂ 1% Nb (w/w), (b) Nb-TiO₂ 2.5% Nb (w/w), (c) Nb-TiO₂ 0% Nb (w/w), (d) Anatase TiO₂, and (e) Nb-TiO₂ 0.5% Nb (w/w).

peaks matched the theoretical frequencies of TiO₂ anatase and that these results also matched with the XRD diffractograms. In contrast, there was a reduction in the intensity of the characteristic peaks at 395, 515, and 638 cm⁻¹, respectively, while the concentration of Nb increased in the photocatalytic powders. This indicated the incorporation of Nb into the TiO₂ lattice, which confirmed the results obtained by XRD and Rietveld.

3.4. Diffuse Reflectance and SBET Characterization. The results of diffuse reflectance spectroscopy using Tauc extrapolation [29] showed values from 3.33 eV to 3.38 eV for the photocatalytic powders Nb-TiO₂ 0.0% (w/w) and Nb-TiO₂ 2.5% (w/w), respectively, indicating that the addition of Nb to the TiO₂ lattice did not increase the bandgap value significantly. The diffuse reflectance results of all photocatalytic powders analysed were similar and close to the value of 3.38 eV, which indicates that the photocatalytic powders modified through sputtering did not able to promote and/or increase the formation of new defects near the conduction band of the photocatalysts when compared with the photocatalysts not modified through sputtering [30] (Figure 7).

The SBET surface area results for the photocatalytic powders are shown in Table 2. The results indicate a gradual increase from 22.6 to 31.6 m²·g⁻¹ in photocatalytic powders Nb-TiO₂ 0.0% Nb (w/w) to Nb-TiO₂ 2.5% Nb (w/w), respectively. A similar behavior was observed in photocatalytic powders modified by deposition of Nb⁰ through sputtering. A

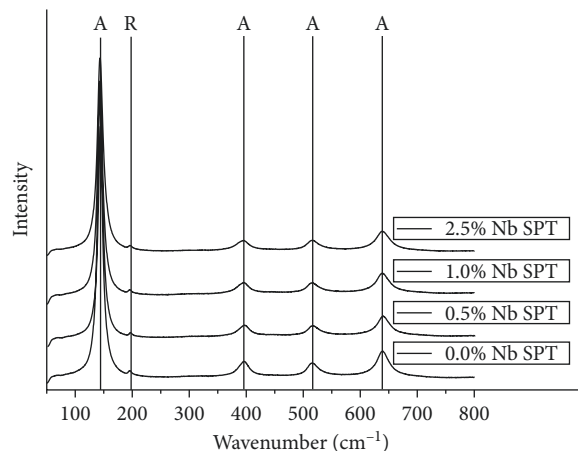


FIGURE 6: Raman spectra of the photocatalytic powders modified by deposition of Nb⁰ through sputtering (A, anatase; R, rutile peaks).

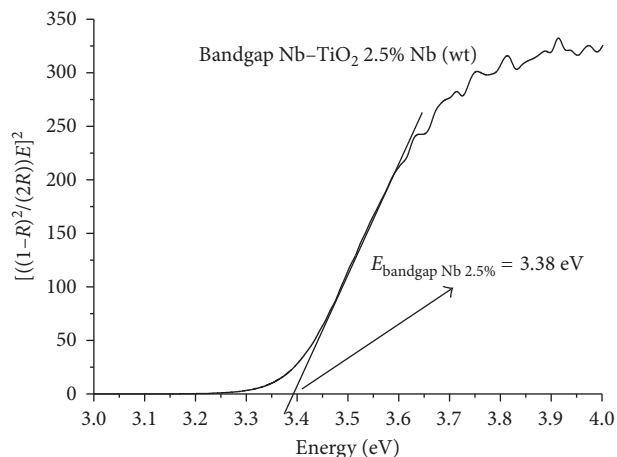


FIGURE 7: Bandgap (Tauc extrapolation) graph of Nb-TiO₂ 2.5% Nb (w/w) photocatalytic powder.

slight increase in the surface area of photocatalytic powders was observed, which is justified by the presence of deposited Nb⁰, which can act as a deagglomerator of particles due to the electrostatic repulsion effect, which increases the surface area.

3.5. SEM Characterization. The SEM images obtained of the photocatalytic powder Nb-TiO₂ 0.0% Nb (w/w) without modification, by deposition of Nb⁰ through sputtering, are illustrated in Figure 8. All the compositions (with or without

TABLE 2: Surface area and average particle size of the synthesized photocatalytic powders.

Photocatalyst (% Nb (w/w))	SBET area ($\text{m}^2 \cdot \text{g}^{-1}$)	Average particle size (nm)	Photocatalyst (% Nb (w/w))	SBET area ($\text{m}^2 \cdot \text{g}^{-1}$)	Average particle size (nm)
Nb-TiO ₂ 0.0%	22.6	15	Nb-TiO ₂ 0.0% SPT	25.8	15
Nb-TiO ₂ 0.5%	23.4	15	Nb-TiO ₂ 0.5% SPT	28.2	14
Nb-TiO ₂ 1.0%	32.6	15	Nb-TiO ₂ 1.0% SPT	37.3	14
Nb-TiO ₂ 2.5%	31.6	13	Nb-TiO ₂ 2.5% SPT	37.2	13

SPT: modification through sputtering.

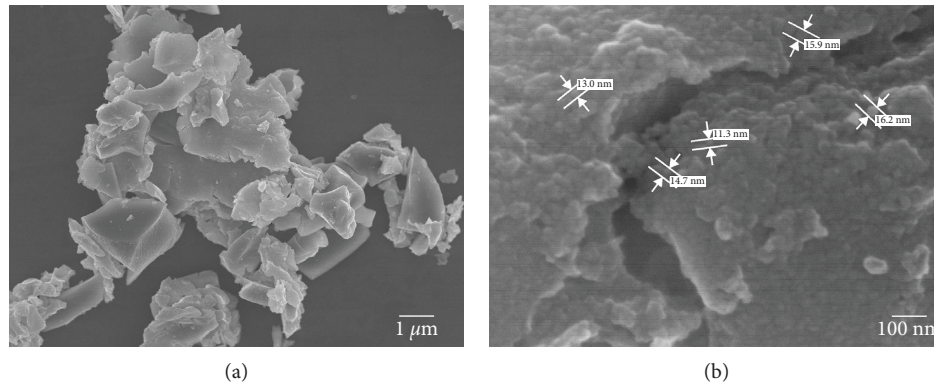


FIGURE 8: SEM images of photocatalytic powder Nb-TiO₂ 0.0% Nb (w/w) without modification by deposition of Nb⁰ through sputtering. Different magnifications.

surface modification) showed similar microstructures. It was found that the photocatalytic powders are formed by plates of irregular shapes and sizes, ranging from 1 to 7 μm as seen in Figure 8(a). They are composed of clusters of rounded particles with diameters between 11.3 and 16.2 nm, as shown in Figure 8(b).

3.6. XPS Characterization. The XPS technique was used to analyze the chemical surface structure of the photocatalytic powders and verify changes in chemical composition that happened due to the substitution of Ti for Nb. In the XPS spectra on the Ti_{2p} transition, Figure 9(a), the oxidation state of titanium Ti⁴⁺ is represented by the characteristic peak of Ti_{2p} (458.5 eV) and the Nb substitution not resulted in modification of the TiO₂ oxidation original state. Regarding Nb (Figure 9(b)) represented by characteristic peaks NbO_{2 3d3/2}-Nb⁴⁺ in 209.5 eV, NbO_{2 3d5/2}-Nb⁴⁺ in 206.7 eV, and Nb₂O₅ in 207.4 \pm 0.4 eV, it was observed that the oxidation state of niobium in the photocatalytic powders is Nb⁴⁺. However, this paper was based on the fact that the Nb replaced in the TiO₂ crystalline lattice is found in the oxidation state 5+. If that should happen, an electron donor level could be generated in the forbidden region of the bandgap, which would be easily removed, becoming a free electron promoted and used in the reaction of CO₂ reduction.

The substitution of Ti⁴⁺ for Nb⁵⁺ is a subject for further studies which will evaluate the influence of temperatures higher than 500°C in the presence of an oxidizing atmosphere and the Nb oxidation state behavior replaced by TiO₂ lattice. Furthermore, the phase transition anatase/rutile

seeking favorable conditions for the formation of Nb⁵⁺ and avoiding the formation of the rutile crystalline phase as much as possible will be observed.

3.7. CO₂ Reduction Assays. The results of the CO₂ reduction and the formation of methanol, as shown in Table 3, indicate that the addition of structural Nb favored the formation of methanol. It was found that the photocatalytic powder Nb-TiO₂ 0.0% Nb (w/w) did not promote the formation of methanol, and the surface modification through sputtering showed lower results in comparison with the powders not modified by this technique. The concentrations of methanol obtained can be explained by XPS wherein Nb replaced was Nb⁴⁺ instead of Nb⁵⁺. If the replacement by Nb⁵⁺ occurs in the lattice of TiO₂, this replacement can lead to a level of electron donation that could be used in reduction reaction; however, the substitution by Nb⁴⁺ can act in the reduction reaction in the same way, but with lower activity expected, once there is no remaining electron. The concentration of methanol formed is directly proportional to the Nb concentration in the powders, and the formation of methanol is due to the presence of Nb in the lattice of TiO₂. Concerning the formation of metallic antennae, the reaction of reduction occurs in some preferential sites, and those sites can be covered by the sputtered antennae decreasing photocatalytic activity and the methanol formation when compared with same powders not modified through sputtering. The yield of methanol reached by catalyst Nb-TiO₂ 2.5% (w/w) (1.00 $\mu\text{mol/g}\cdot\text{cat}\cdot\text{h}$) is superior in comparison with all the catalysts but P25 (1.83 $\mu\text{mol/g}\cdot\text{cat}\cdot\text{h}$), demonstrating the doping with Nb⁴⁺, has potential effect in formation of defects

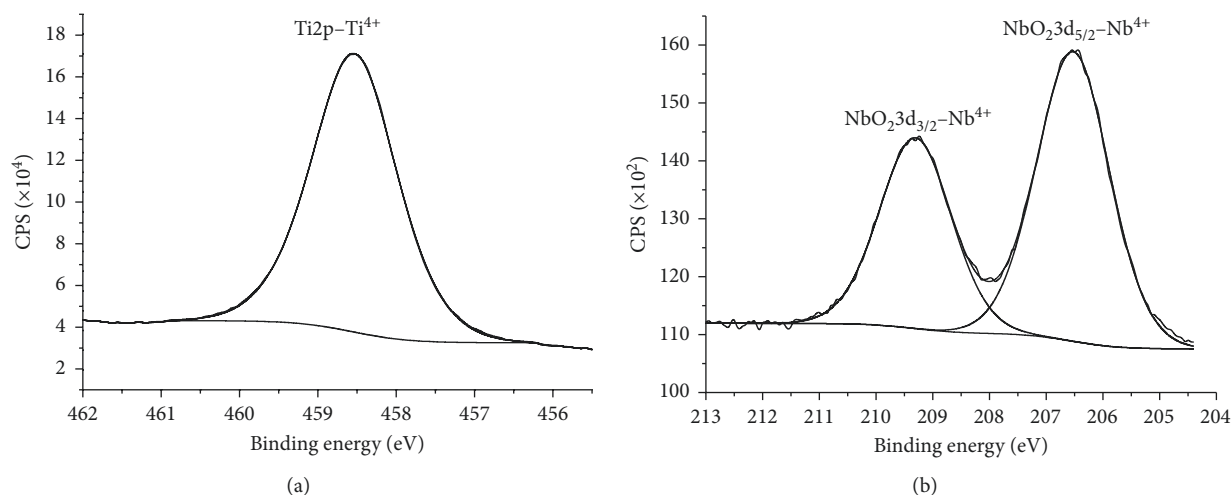


FIGURE 9: XPS spectra of Nb-TiO₂ 2.5% Nb (w/w) photocatalyst: (a) Ti_{2p} peaks and (b) NbO₂ 3d_{3/2} NbO₂ 3d_{5/2} peaks.

TABLE 3: Methanol concentrations obtained, quantified by GC-FID.

Photocatalytic powder (% Nb (w/w))	Methanol yield ($\mu\text{mol/g-cat-h}$)	Photocatalytic powder (% Nb (w/w))	Methanol yield ($\mu\text{mol/g-cat-h}$)
Blank (photolysis)	0	P25	1.83
Nb-TiO ₂ 0.0%	0	Nb-TiO ₂ 0.0% SPT	0
Nb-TiO ₂ 0.5%	0.54	Nb-TiO ₂ 0.5% SPT	<0.01
Nb-TiO ₂ 1.0%	0.76	Nb-TiO ₂ 1.0% SPT	0.16
Nb-TiO ₂ 2.5%	1.00	Nb-TiO ₂ 2.5% SPT	0.40

which increases the electron-hole pair recombination time improving the catalytic properties of TiO₂.

As discussed above, the formation of methanol is directly proportional to Nb concentration which can open new promising researches to investigate higher concentrations (above 2.5%) of Nb that can reach yields of methanol equal or higher than P25.

4. Conclusions

We obtained nanostructured TiO₂ photocatalytic powders structurally modified with Nb using the Pechini method and superficially modified with Nb⁰ through sputtering. The photocatalytic powders are mainly formed by the anatase phase of TiO₂. Utilizing the Rietveld technique, the $\Delta 2\theta^\circ$ displacement peaks, observed by the XRD measurement, confirmed the replacement of Ti for Nb in the TiO₂ lattice. Using SEM, the experiment investigated the morphology of the photocatalytic powders, which were arranged in plates formed by nanosized particles. The SBET technique showed that the surface area of the photocatalytic powders tends to increase with the concentration of Nb. Followed by the reduction of agglomerate formation. The diffuse reflectance technique quantified the average value of bandgap at 3.35 eV. The XPS indicated that the oxidation state of Ti and Nb in the photocatalytic powders is 4+. The substitution to Nb⁰ through sputtering does not increase photoactivity compared to photocatalytic powders with the same concentration of Nb not modified through sputtering. This is justified by the metallic particles of Nb that assist in the

transportation of photogenerated electrons. The formation of methanol was proved by GC-FID in which concentrations up to 1.00 $\mu\text{mol/g-cat-h}$ were obtained by the replacement of Ti⁴⁺ by Nb⁴⁺ in the lattice of TiO₂. Future investigations about higher concentrations of Nb can lead to reach yields of methanol equal or higher than P25.

Conflicts of Interest

The authors declare that they have no conflicts of interest.

Acknowledgments

The authors thank the LMA-IQ for providing the FEG-SEM facilities and also thank the Brazilian research funding agencies CAPES, CNPq, and FAPESP (2008/544136-R) and FAPESP-CDMF (2013/07296-2) for providing the financial support of this research project.

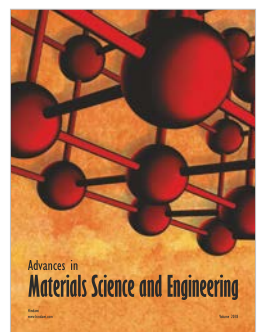
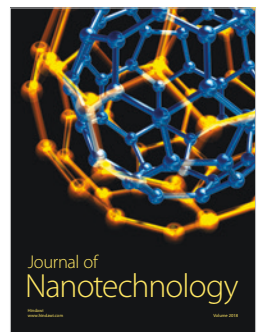
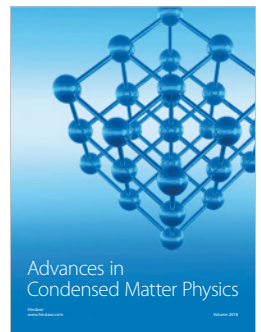
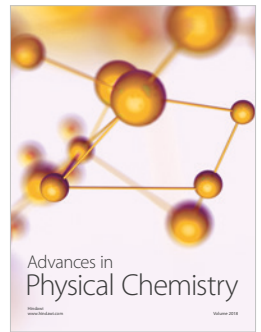
References

- [1] A. Fujishima and K. Honda, "Electrochemical photolysis of water at a semiconductor electrode," *Nature*, vol. 238, no. 5358, pp. 37-38, 1972.
- [2] Q. Gui, Z. Xu, H. Zhang et al., "Enhanced photoelectrochemical water splitting performance of anodic TiO₂ nanotube arrays by surface passivation," *ACS Applied Materials & Interfaces*, vol. 6, no. 19, pp. 17053-17058, 2014.
- [3] G. L. Chiarello, A. Zuliani, D. Ceresoli, R. Martinazzo, and E. Selli, "Exploiting the photonic crystal properties of TiO₂

- nanotube arrays to enhance photocatalytic hydrogen production,” *ACS Catalysis*, vol. 6, no. 2, pp. 1345–1353, 2016.
- [4] M. Nolan, A. Iwaszuk, A. K. Lucid, J. J. Carey, and M. Fronzi, “Design of novel visible light active photocatalyst materials: surface modified TiO₂,” *Advanced Materials*, vol. 28, no. 27, pp. 5425–5446, 2016.
- [5] T. E. Rosser, C. D. Windle, and E. Reisner, “Electrocatalytic and solar-driven CO₂ reduction to CO with a molecular manganese catalyst immobilized on mesoporous TiO₂,” *Angewandte Chemie*, vol. 128, no. 26, pp. 7514–7518, 2016.
- [6] T. Ohno, K. Sarukawa, K. Tokieda, and M. Matsumura, “Morphology of a TiO₂ photocatalyst (Degussa, P-25) consisting of anatase and rutile crystalline phases,” *Journal of Catalysis*, vol. 203, no. 1, pp. 82–86, 2001.
- [7] M. F. Abdel-Messih, M. A. Ahmed, and A. S. El-Sayed, “Photocatalytic decolorization of Rhodamine B dye using novel mesoporous SnO₂-TiO₂ nano mixed oxides prepared by sol-gel method,” *Journal of Photochemistry and Photobiology A: Chemistry*, vol. 260, pp. 1–8, 2013.
- [8] S. M. Lam, J. C. Sin, A. Z. Abdullah, and A. R. Mohamed, “Degradation of wastewaters containing organic dyes photocatalysed by zinc oxide: a review,” *Desalination and Water Treatment*, vol. 41, no. 1–3, pp. 131–169, 2012.
- [9] J. C. Sin, S. M. Lam, A. R. Mohamed, and K. T. Lee, “Degrading endocrine disrupting chemicals from wastewater by TiO₂ photocatalysis: a review,” *International Journal of Photoenergy*, vol. 2012, Article ID 185159, 23 pages, 2012.
- [10] H. Jaafar, Z. A. Ahmad, and M. F. Ain, “Effect of Nb-doped TiO₂ photoanode using solid state method with *E. conferta* as sensitizer on the performance of dye sensitized solar cell,” *Optik-International Journal for Light and Electron Optics*, vol. 144, pp. 91–101, 2017.
- [11] L. Matějová, M. Šihor, J. Lang et al., “Investigation of low Ce amount doped-TiO₂ prepared by using pressurized fluids in photocatalytic N₂O decomposition and CO₂ reduction,” *Journal of Sol-Gel Science and Technology*, vol. 84, no. 1, pp. 158–168, 2017.
- [12] L. Perazolli, G. F. Pegler, M. R. A. Silva, R. A. F. Ingino, and J. A. Varela, “High activity photocatalyst powder formed by three ceramic oxides,” *Advances in Science and Technology*, vol. 65, pp. 184–193, 2010.
- [13] J. Li, X. Xu, X. Liu, W. Qin, M. Wang, and L. Pan, “Metal-organic frameworks derived cake-like anatase/rutile mixed phase TiO₂ for highly efficient photocatalysis,” *Journal of Alloys and Compounds*, vol. 690, pp. 640–646, 2017.
- [14] P. Zhou, Z. Le, Y. Xie, J. Fang, and J. Xu, “Studies on facile synthesis and properties of mesoporous CdS/TiO₂ composite for photocatalysis applications,” *Journal of Alloys and Compounds*, vol. 692, pp. 170–177, 2017.
- [15] J. Tao, Z. Gong, G. Yao et al., “Enhanced optical and photocatalytic properties of Ag quantum dots-sensitized nanostructured TiO₂/ZnO heterojunctions,” *Journal of Alloys and Compounds*, vol. 688, pp. 605–612, 2016.
- [16] I. Ganesh, “Conversion of carbon dioxide into methanol—a potential liquid fuel: fundamental challenges and opportunities (a review),” *Renewable and Sustainable Energy Reviews*, vol. 31, pp. 221–257, 2014.
- [17] N. Li, M. Liu, B. Yang et al., “Enhanced photocatalytic performance toward CO₂ hydrogenation over nanosized TiO₂-loaded Pd under UV irradiation,” *Journal of Physical Chemistry C*, vol. 121, no. 5, pp. 2923–2932, 2017.
- [18] M. Cheng, S. Yang, R. Chen, X. Zhu, Q. Liao, and Y. Huang, “Copper-decorated TiO₂ nanorod thin films in optofluidic planar reactors for efficient photocatalytic reduction of CO₂,” *International Journal of Hydrogen Energy*, vol. 42, no. 15, pp. 9722–9732, 2017.
- [19] Y. X. Pan, Z. Q. Sun, H. P. Cong et al., “Photocatalytic CO₂ reduction highly enhanced by oxygen vacancies on Pt-nanoparticle-dispersed gallium oxide,” *Nano Research*, vol. 9, no. 6, pp. 1689–1700, 2016.
- [20] G. M. M. M. Lustosa, J. P. C. Costa, L. A. Perazolli, B. D. Stojanovic, and M. A. Zaghete, “Electrophoretic deposition of (Zn, Nb)SnO₂-films varistor superficially modified with Cr³⁺,” *Journal of the European Ceramic Society*, vol. 35, no. 7, pp. 2083–2089, 2015.
- [21] M. P. Pechini, “Method of preparing lead and alkaline titanates and niobates and coating method using the same to form a capacitor,” US Patent 3330697, 1967.
- [22] K. Safeen, V. Micheli, R. Bartali et al., “Synthesis of conductive and transparent Nb-doped TiO₂ films: role of the target material and sputtering gas composition,” *Materials Science in Semiconductor Processing*, vol. 66, pp. 74–80, 2017.
- [23] A. V. Manole, M. Dobromir, M. Girtan, R. Mallet, G. Rusu, and D. Luca, “Optical properties of Nb-doped TiO₂ thin films prepared by sol-gel method,” *Ceramics International*, vol. 39, no. 5, pp. 4771–4776, 2013.
- [24] E. E. Nikishina, D. V. Drobot, and E. N. Lebedeva, “Niobium and tantalum: state of the world market, application fields, and sources of raw materials. Part 2,” *Russian Journal of Non-Ferrous Metals*, vol. 55, no. 2, pp. 130–140, 2014.
- [25] X. Cheng, Z. Li, and J. Wu, “Colossal permittivity in ceramics of TiO₂ Co-doped with niobium and trivalent cation,” *Journal of Materials Chemistry A*, vol. 3, no. 11, pp. 5805–5810, 2015.
- [26] P. D. Spagnol, J. A. Varela, M. A. Z. Bertochi, B. D. Stojanovic, and S. M. Tebcherani, “Effect of precursor solution on the formation of perovskite phase of Pb(Mg_{1/3}Nb_{2/3})O₃ thin films,” *Thin Solid Films*, vol. 410, no. 1–2, pp. 177–182, 2002.
- [27] C. J. Tavares, M. V. Castro, E. S. Marins et al., “Effect of hot-film annealing in a hydrogen atmosphere on the electrical and structural properties of Nb-doped TiO₂ sputtered thin films,” *Thin Solid Films*, vol. 520, no. 7, pp. 2514–2519, 2012.
- [28] I. Tseng, W. Chang, and J. C. S. Wu, “Photoreduction of CO₂ using sol-gel derived titania and titania-supported copper catalysts,” *Applied Catalysis B: Environmental*, vol. 37, no. 1, pp. 37–48, 2002.
- [29] D. L. Wood and J. Tauc, “Weak absorption tails in amorphous semiconductors,” *Physical Review B*, vol. 5, no. 8, pp. 3144–3151, 1972.
- [30] A. Kubacka, G. Colón, and M. Fernandez-García, “Cationic (V, Mo, Nb, W) doping of TiO₂-anatase: a real alternative for visible light-driven photocatalysts,” *Catalysis Today*, vol. 143, no. 3–4, pp. 286–292, 2009.



Hindawi
Submit your manuscripts at
www.hindawi.com



Copyright of Advances in Materials Science & Engineering is the property of Hindawi Limited and its content may not be copied or emailed to multiple sites or posted to a listserv without the copyright holder's express written permission. However, users may print, download, or email articles for individual use.